Available online at www.elixirpublishers.com (Elixir International Journal)

Computer Engineering

Elixir Comp. Engg. 137 (2019) 53905-53910

ISSN: 2229-712X

Medical Image Fusion using Undecimated Discrete Wavelet Transform for Analysis and Detection of Alzheimer's Disease

T.Tirupal, T.K.Naga Vaishnavi, K.Anitha, K.Lavanya and E.H.Sandhya
Department of ECE, G.Pullaiah College of Engineering and Technology, Kurnool, India

ARTICLE INFO

Article history:
Received: 4 November 2019;
Received in revised form:
25 November 2019;
Accepted: 5 December 2019;

Keywords
Fusion,
UDWT,
Modified Spatial Frequency,
PSNR.

ABSTRACT

A novel algorithm for effectively fusing Alzheimer's effected medical images is proposed in this paper. Fusing is done in the Undecimated Discrete Wavelet Transform (UDWT) domain. Firstly, the RGB images are converted in to NTSC images and then UDWT is applied. In UDWT domain, Low frequency subbands are fused using maximum selection rule and high frequency subbands are fused according to the Modified Spatial Frequency (MSF). Lastly, fused image is obtained by inverse UDWT. The fused NTSC is again converted in to RGB image for fused RGB image. Superiority of the proposed method is presented and justified. Fused image quality is verified with various quality metrics i.e., Peak Signal to Noise Ratio (PSNR), Entropy, Spatial Frequency (SF) etc.,

Introduction

Alzheimer's disease is the most common form of dementia [1,2,3] in people. Alzheimer's disease (AD) [4, 5, 6] is an irreversible disease of the brain that affects a person's memory, thinking, and other abilities. The disease is named after Dr.Alois Alzheimer. In 1906, Dr. Alzheimer noticed changes in the brain tissue of a woman who had died of an unusual mental illness. Her symptoms included memory loss, language problems, and unpredictable behaviour. After she died, he examined her brain and found many abnormal clumps (now called amyloid plaques) and tangled bundles of fibers (now called neurofibrillary, or tau tangles). Figure 1 shows the brain affected image by Alzheimer's disease.

Figure 1. Brain affected by Alzheimer's disease

Types of Alzheimer's disease [7, 8]

Early-onset Alzheimer's: This type happens to people who are younger than age 65. Often, they're in their 40s or 50s when they're diagnosed with the disease. It's rare -- up to 5% of all people with Alzheimer's have early-onset. People with Down syndrome have a higher risk for it.

Late-onset Alzheimer's: This is the most common form of the disease, which happens to people age 65 and older. It may or may not run in families. So far, researchers haven't found a particular gene that causes it. No one knows for sure why some people get it and others don't.

Classification of Alzheimer's disease [9, 10, 11]

Sporadic: It is caused due to genetic and environmental risk factors. 90-95% of cases are recorded under sporadic. 50% cases are related to age 85.Only 1% cases are related to 60-65 age.

Familial: It is caused due to mutations in gene.5-10% cases are recorded under familial. More than two people from a family must have alzheimer's disease to fall under this kind.

Stages of Alzheimer's disease [12, 13, 14]

Stage 1: normal: There are no symptoms at this stage but there might be an early diagnosis based on family history.

Stage 2: normal aged forget fullness: The earliest symptoms appear, such as forgetfulness.

Stage 3: mild cognitive impairment: Mild physical and mental impairments appear, such as reduced memory and concentration. These may only be noticeable by someone very close to the person.

Stage 4: mild Alzheimer's: Alzheimer's is often diagnosed at this stage, but it's still considered mild. Memory loss and the inability to perform everyday tasks is evident.

Stage 5: moderate Alzheimer's: Moderate to severe symptoms require help from loved ones or caregivers.

Stage 6: moderately severe Alzheimer's: At this stage, a person with Alzheimer's may need help with basic tasks, such as eating and putting on clothes.

Stage 7: severe Alzheimer's disease:-This is the most severe and final stage of Alzheimer's. There may be a loss of speech and facial expressions.

Symptoms of Alzheimer's disease [15, 16, 17, 18]

Everyone has episodes of forgetfulness from time to time. But people with Alzheimer's disease display certain on-going behaviours and symptoms that worsen over time.
These can include:

- Memory loss affecting daily activities, such as an ability to keep appointments
- Trouble with familiar tasks, such as using a microwave
- Difficulties with problem-solving
- Trouble with speech or writing

Tele: +919491236447
E-mail address: tirutalari@gmail.com

- Becoming disoriented about times or places
- Decreased judgment
- Decreased personal hygiene
- Mood and personality changes
- Withdrawal from friends, family, and community
- Symptoms change according to the stage of the disease.

Undecimated Discrete Wavelet Transform

The Discrete Wavelet Transform (DWT) [19, 20, 21, 22] is referred to as Mallat's algorithm, which is based on orthogonal decomposition of the image onto a wavelet basis in order to avoid the redundancy of information in the pyramid at each level of resolution. Consequently, Undecimated Discrete Wavelet Transform (UDWT) [23, 24, 25, 26, 27, 28] avoids image decimation which has been developed for image processing applications such as denoising [29], texture classification [30, 31], pattern recognition and fusion [32, 33, 34, 35, 36, 37, 38]. The discrete implementation of UDWT can be accomplished by using the 'a trous' (with holes) algorithm, which presents interesting properties such as:

The evaluation of the wavelet decomposition can be followed from level to level.

A single wavelet coefficient plane is produced at each level of decomposition.

The wavelet coefficients are computed for each location allowing a better detection of dominant feature.

It is easily implemented.

The 'a trous' wavelet transform is a non-orthogonal multiresolution decomposition, which separates the low-frequency information (approximation) from high-frequency information (detail coefficients). Such a separation uses a low-pass filter $h(n)$, associated with the scale function $\varphi(x)$, to obtain successive approximations of a signal through scales as follows:

$$a_j(k)=\sum_n h(n)a_{j-1}(k+n2^{j-1}), \quad j=1,....,N \tag{1}$$

Where $a_0(k)$ corresponds to the original discrete signal $s(k)$; j and N are the scale index and the number of scales, respectively.

The wavelet coefficients are extracted by using a high-pass filter $g(n)$, associated with the wavelet function $\psi(x)$, through the following filtering operation

$$w_j(k)=\sum_n g(n)a_{j-1}(k+n2^{j-1}) \tag{2}$$

The perfect reconstruction of data is performed by introducing two dual filters $hr(n)$ and $gr(n)$ that should satisfy the quadrature mirror filter condition

$$\sum_n hr(n)h(l-n)+gr(n)g(l-n)=\delta(l) \tag{3}$$

Where $\delta(l)$ is the Dirac function. A simple choice consists in considering $hr(n)$ and $gr(n)$ filters as equal to Dirac function $(hr(n)=gr(n)=\delta(n))$. Therefore $g(n)$ is deduced from (3) as

$$g(n)=\delta(n)-h(n) \tag{4}$$

Hence, the wavelet coefficients are obtained by a simple difference between two successive approximations as follows

$$w_j(k)=a_{j-1}(k)-a_j(k) \tag{5}$$

To construct the sequence, this algorithm performs successive convolutions with a filter obtained from an auxiliary function named as the scaling function. Given an image I, the sequence of approximations are constructed are as follows

$$A_1=F(I), \quad A_2=F(A_1), \quad A_3=F(A_2) \tag{6}$$

Where F is a scale function. A B3 cubic spline function is often used for the characterization of the scale function [16] and the use of a B3 cubic spline leads to a convolution with a mask of 5X5

$$\frac{1}{256}\begin{bmatrix}1 & 4 & 6 & 4 & 1\\ 4 & 16 & 24 & 16 & 4\\ 6 & 24 & 36 & 24 & 6\\ 4 & 16 & 24 & 16 & 4\\ 1 & 4 & 6 & 4 & 1\end{bmatrix} \tag{7}$$

As stated above, the wavelet planes are computed as the difference between two consecutive approximations A_{j-1} and A_j. Letting

$$d_j=A_{j-1}-A_j, \qquad j=1,.....,n \tag{8}$$

In which $A_0=I$, the reconstruction formula is

$$I=\sum_{j=1}^{J}d_j+A_J \tag{9}$$

In this representation, the images $A_j(j=0,1,....,J)$ are approximations of the original image I at increasing scales (decreasing resolution levels), $d_j(j=1,........,J)$ are the multiresolution wavelet planes and A_J is a residual image. Note that the original image A_0 has double resolution than A_1, the image A_1 double resolution than A_2 and so on. However, all the consecutive approximations (and wavelet planes) in this process have the same number of pixels as the original image. This is a consequence of the fact that the 'a trous' algorithm is a non-orthogonal oversampled transform.

Proposed Medical Image Fusion Method

In this section, a new method for medical image fusion is proposed, which combines the aspects of low frequency subbands (LFSs) and high frequency subbands (HFSs) using different fusion schemes. The main objective of this paper is to fuse the medical images in which the characteristics of the images should also be considered. From fig. 2 the MRI image provides clear soft tissues information while SPECT provides 3D soft tissue information.

Fusing Low Frequency Subbands using Maximum Selection Rule

The LFSs coefficients are fused using maximum selection rule. According to this fusion rule, the frequency coefficients with greater absolute value are selected as fused coefficients which are shown in equation (10).

$$LFS_F=\begin{cases}LFS_i^X & if\ LFS_i^X\geq LFS_i^Y\\ LFS_i^Y & otherwise\end{cases} \tag{10}$$

Where X and Y are two source images and F is the fused coefficient image. LFS_F is the fused LFS image; LFS_i^x and LFS_i^y are the low frequency subbands of ith region of LFS image for X and Y images respectively.

Fusing High Frequency Subbands using Modified Spatial Frequency

Spatial frequency (SF) proposed by Eskicioglu et al. is calculated by row and column frequency. It reflects the whole activity level of an image and reflects detailed differences and texture changes, which means the larger the SF, the higher the image resolution. We have used a modified version of SF in the proposed image fusion method. Modified Spatial Frequency (MSF) consists of row frequency (RF), column frequency (CF) and diagonal frequency (DF). For an $m\,x\,n$ image F, the MSF is defined as

$$MSF = \sqrt{(RF)^2 + (CF)^2 + (DF)^2} \quad (11)$$

Where,

$$RF = \sqrt{\frac{1}{mn}\sum_{i=1}^{m}\sum_{j=2}^{n}\left[F(i,j) - F(i,j-1)\right]^2} \quad (12)$$

$$CF = \sqrt{\frac{1}{mn}\sum_{i=2}^{m}\sum_{j=1}^{n}\left[F(i,j) - F(i-1,j)\right]^2} \quad (13)$$

And,

$$DF = P + Q \quad (14)$$

Where,

$$P = \sqrt{\frac{1}{mn}\sum_{i=2}^{m}\sum_{j=2}^{n}\left[F(i,j) - F(i-1,j-1)\right]^2} \quad (15)$$

$$Q = \sqrt{\frac{1}{mn}\sum_{i=2}^{m}\sum_{j=2}^{n}\left[F(i-1,j) - F(i,j-1)\right]^2} \quad (16)$$

Algorithm

Figure 2 shows the schematic diagram of the proposed medical image fusion method. The fusion process is accomplished by the following steps:

1. The source medical images A and B are converted to gray images by using NTSC.
2. Now the new images are decomposed by UDWT at level 1 to get LFSs and HFSs.
3. The coefficients of LFSs are fused to get fused LFS using the maximum selection rule described in the above section.
4. The coefficients of HFSs of two source images are segmented into several regions.
5. The modified spatial frequency of corresponding regions of segmented HFSs of two source images is computed as described in the above section.
6. Compare the modified spatial frequency of corresponding regions of two source images to decide which should be used to construct the fused HFS image.

$$HFS_F = \begin{cases} HFS_i^X & if \;\; MSF_i^X > MSF_i^Y \\ HFS_i^Y & otherwise \end{cases} \quad (17)$$

Where HFS_F is the fused HFS image, MSF_i^X and MSF_i^Y are the modified spatial frequencies of the ith region of HFS image for X and Y images respectively.

7. The fused gray image is obtained by performing inverse undecimated discrete wavelet transform on the fused LFSs and HFSs.
8. Now we apply colour transformation to convert the gray image into colour image.
9. The final fused image is an RGB image

Experimental Results and Comparisons

The performance of proposed medical image fusion method on various medical images is presented. The first example is shown in Fig. 3 which contains different output images of different scans. Figs. 3a and b are two medical images of MRI and SPECT [39, 40]. Fig. 3c is the fused image by proposed method. Figs. 4a and b are MRI and SPECT with alzheimer's prove that the proposed method produces better medical information. Figures 5a and b are input images of Type-3. We use the biorthogonal' bior6.8, with a decomposition level of 1, as the wavelet basis for the proposed method. Experimental results on several pairs of medical images of MRI and SPECT with alzheimer's disease [41] prove that the proposed method produces better medical information. For further comparison of fusion results the following objective fidelity criteria are used and the values of all objective criteria [42, 43] are listed in Table 1 for figs. 3, 4 and 5.

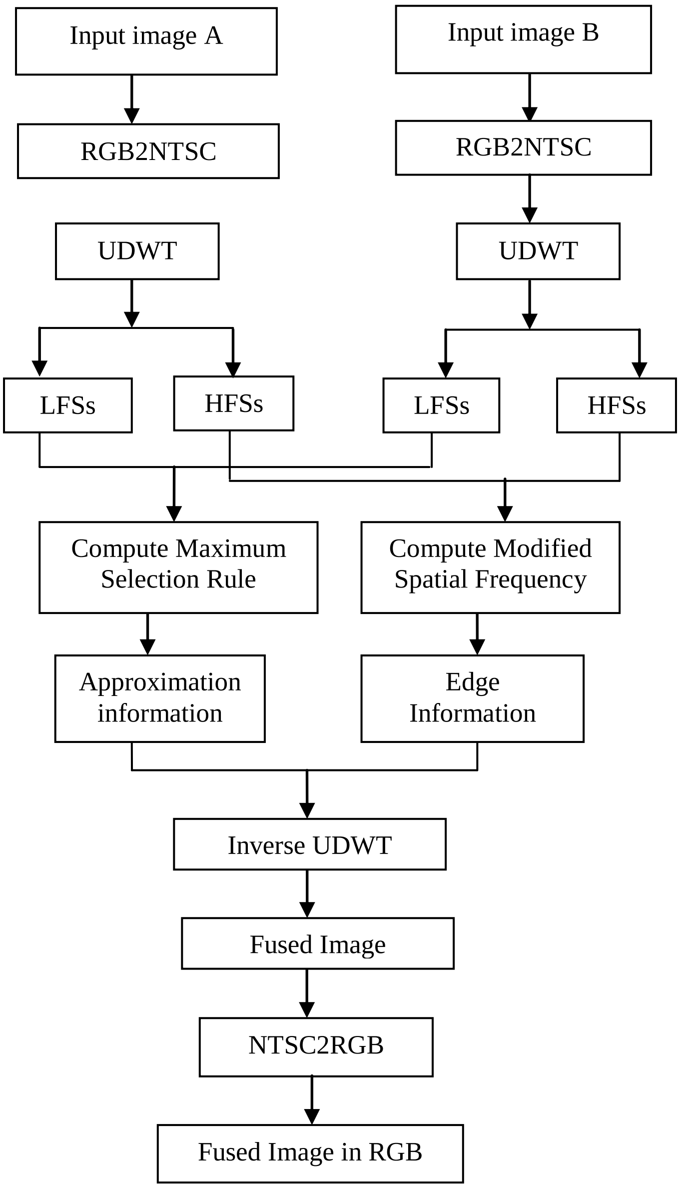

Figure 2. Schematic diagram of the proposed method

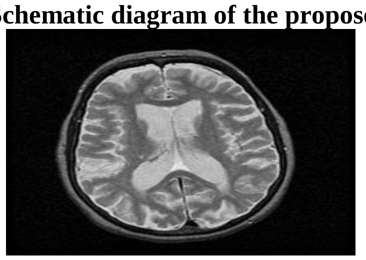

(a)

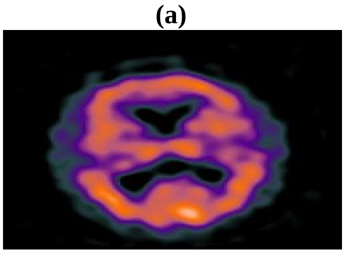

(b)

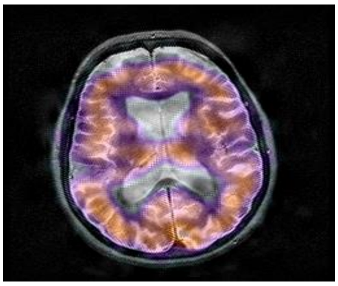

(c)

Figure 3. Fusion results for Type-1 MRI and SPECT images (a) MRI image (b) SPECT image (c) Fused image by the proposed method.

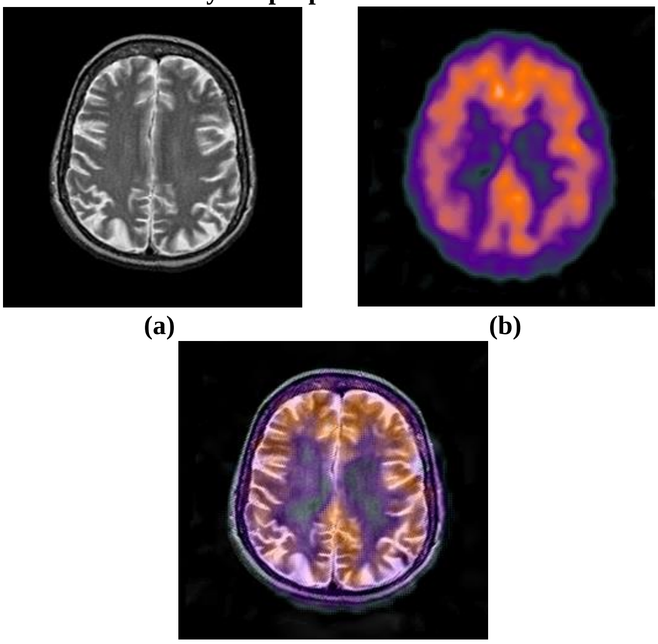

(a) (b) (c)

Figure 4. Fusion results for Type-2 MRI and SPECT images (a) MRI image (b) SPECT image (c) Fused image by the proposed method

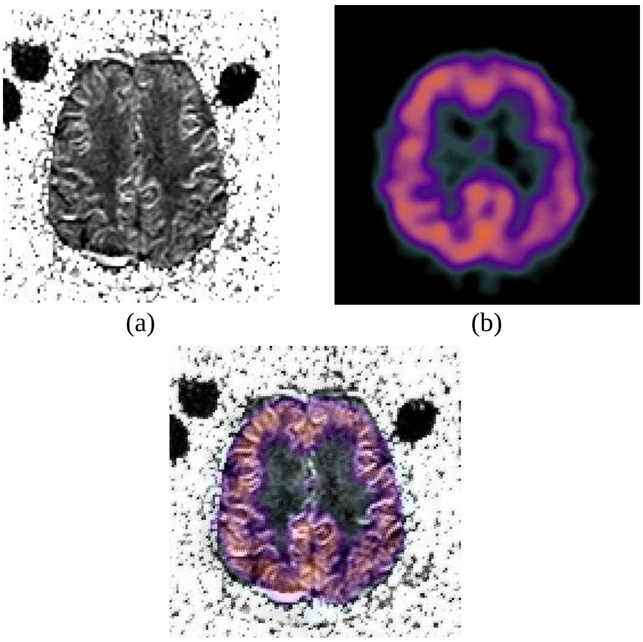

(a) (b) (c)

Figure 5. Fusion results for Type-3 MRI and SPECT images (a) MRI image (b) SPECT image (c) Fused image by the proposed method

Table 1. Performance evaluation results for different types of MRI and SPECT images.

MRI-SPECT	PSNR (dB)	Entropy (bits/symbol)	Average Pixel Intensity	SF (Cycles/ millimeter)	SD
Type-1	64.67	6.47	0.23	23.43	0.28
Type-2	67.13	5.71	0.20	20.00	0.26
Type-3	54.41	6.77	0.65	60.94	0.34

Spatial Frequency (SF)

It is a metric which measures the overall activity level of an image and reflects detailed differences and texture changes. For an $m\,x\,n$ image Z, the SF [20] is defined as

$$SF = \sqrt{(RF)^2 + (CF)^2} \tag{18}$$

Where *RF* and *CF* are row frequency and column frequency respectively

$$RF = \sqrt{\frac{1}{mn}\sum_{i=1}^{m}\sum_{j=2}^{n}\left[Z(i,j) - Z(i,j-1)\right]^2} \tag{19}$$

$$CF = \sqrt{\frac{1}{mn}\sum_{i=2}^{m}\sum_{j=1}^{n}\left[Z(i,j) - Z(i-1,j)\right]^2} \tag{20}$$

The larger the value of *SF*, the better the fusion result.

Entropy (H)

Entropy is used to measure the information content of an image. Entropy is sensitive to noise and other unwanted rapid fluctuations. An image with high information content would have high entropy. It is defined as:

$$H = -\sum_{i=0}^{L} h_{I_f}(i)\log_2 h_{I_f}(i) \tag{21}$$

Where $h_{I_f}(i)$ the normalized histogram of the fused image and L is the number of frequency bins in the histogram.

Peak Signal to Noise Ratio (PSNR)

The peak signal to noise ratio is the ratio between the maximum value of an image and the magnitude of background noise and is commonly used as a measure of quality of reconstruction in image fusion. It is defined as:

$$PSNR = 10\log_{10}\left(\frac{L^2}{\frac{1}{MN}\sum_{i=1}^{M}\sum_{j=1}^{N}(I_r(i,j) - I_f(i,j))^2}\right) \quad 22)$$

Where *L* is the number of gray levels in the image (here, *L=255*). Higher *PSNR* implies better is the quality of fused image.

Standard Deviation (SD)

Standard deviation is a measure of the dispersion of a set of data from its mean. It is calculated as the square root of variance by determining the variation between each data point relative to the mean. If the data points are further from the mean, there is higher deviation within the dataset. The standard deviation of an entire population is known as (sigma) and is calculated using summation (or total), and N is the number of values in the population.

Average Pixel Intensity

A pixel (short for picture element) is a small block that represents the amount of gray intensity to be displayed for that particular portion of the image. For most images, pixel values are integers that range from 0 (black) to 255 (white).

Conclusion

In this paper we have discussed a new method for fusing Alzheimer's affected images based on UDWT. The fusion of medical images plays an important role in many clinical applications for they can support more accurate information than any individual image. This paper presents the detection of Alzheimer's disease in the following three steps. In the first step, the Alzheimer's affected images MRI and SPECT RGB images are converted in to NTSC image and are decomposed into sub images by UDWT. In the second step the coefficients of low-frequency band are fused using maximum selection rule and the coefficients of high-frequency band are fused using modified spatial frequency. In the last step, the fused image is constructed by the inverse UDWT with the composite coefficients and then the obtained NTSC image is again converted in to RGB image. The performance of the proposed method proves its accuracy and strength over different image fusion techniques with the help of visual and quantitative measures.

References

[1] World Alzheimer Report 2018, "The state of the art of dementia research: New frontiers," Published by Alzheimer's Disease International (ADI), London, September 2018.

[2] Alzheimer's Association Report, "2017 Alzheimer's disease facts and figures," Alzheimer's & Dementia, pp. 1–49, 2017, doi.org/10.1016/j.jalz.2017.02.001.

[3] Dalcerri M, Garcia A, McKiel H, "Vitamin D Deficiency and the Increased Risk of Developing Dementia and Alzheimer's Disease," J Geriatr Med Res. vol.1 No.1: 03, 2017.

[4] Leilani Doty, "Coconut Oil for Alzheimer's Disease," Clinical Practice, vol. 1(2), pp. 12–17, 2012, doi:10.5923/j.cp.20120102.01.

[5] Samuel, "Recent Research and Updates on Alzheimer's Disease," Journal of Psychology and Behavioral Science, vol. 2 (2), pp. 103–112, June 2014.

[6] Linda R. Struckmeyer, and Noralyn Davel Pickens, "Home modifications for people with Alzheimer's disease: A scoping review," American Journal of Occupational Therapy, vol. 70, 2016, doi:org/10.5014/ajot.2015.016089.

[7] Zenglin Xu, Shandian Zhe, Yuan(Alan) Qi, Peng Yu, "Association Discovery and Diagnosis of Alzheimer's Disease with Bayesian Multiview Learning," Journal of Artificial Intelligence Research, vol. 56, pp. 247–268, 2016.

[8] Zhuo Li, Hua Zhu, Ling Zhang, Chuan Qin, "The intestinal microbiome and Alzheimer's disease: A review," Animal Model Exp Med., vol. 1, pp. 180–188, 2018, doi:10.1002/ame2.12033.

[9] Ambreen Mirza, Andrew King, Claire Troakes, Christopher Exley, "Aluminium in brain tissue in familial Alzheimer's disease," Journal of Trace Elements in Medicine and Biology, vol. 40, pp. 30–36, 2017.

[10] Luis Javier Herrera, Ignacio Rojas, H. Pomares, A. Guillen, O. Valenzuela, O. Banos, "Classification of MRI images for Alzheimer's disease detection," IEEE, 2013 doi:10.1109/SocialCom.2013.127.

[11] Zhe Xiao, Yi Ding, Tian Lan, Cong Zhang, Chuanji Luo, and Zhiguang Qin, "Brain MR Image Classification for Alzheimer's Disease Diagnosis Based on Multifeature Fusion," Computational and Mathematical Methods in Medicine, 2017, doi.org/10.1155/2017/1952373.

[12] Ramesh Kumar Lama, Jeonghwan Gwak, Jeong-Seon Park and Sang-Woong Lee, "Diagnosis of Alzheimer's Disease Based on Structural MRI Images Using a Regularized Extreme Learning Machine and PCA Features," Journal of Healthcare Engineering, 2017, doi.org/10.1155/2017/5485080.

[13] Sahar Y. Al-Okbi, Doha A. Mohamed, Mohamed Abdel Fatah, Kholoud Abdel Aal, Shaimaa E Mohammed, "Evaluation of Plant Food Extracts in Experimental Model of Alzheimer's Like Disease Induced by Aluminum Lactate in Rats," Journal of Applied Pharmaceutical Science, vol. 7 (7), pp. 070–076, July, 2017, doi:10.7324/JAPS.2017.70712.

[14] Stacy Smallfield, Cindy Heckenlaible, "Effectiveness of occupational therapy interventions to enhance occupational performance for adults with Alzheimer's disease and related major neurocognitive disorders: A systematic review," American Journal of Occupational Therapy, vol. 71 (5), 2017, doi:org/10.5014/ajot.2017.024752.

[15] Mohammed Qumani Ahmed, Fahaad S.H. Alenazi, Mohammad Feroze Fazaludeen, S.M.A. Shahid, Mohd Adnan Kausar, "Pathology and Management of Alzheimer's disease: A review," International Journal of Pharmaceutical Research & Allied Sciences, vol. 7 (2), pp. 30–42, 2018.

[16] C. A. Lane, J. Hardy and J. M. Schott, "Alzheimer's disease," European Journal of Neurology, vol. 25, pp. 59–70, 2018, doi:10.1111/ene.13439.

[17] Melinda Kelley, Brigette Ulin, and Lisa C. McGuire, "Reducing the Risk of Alzheimer's Disease and Maintaining Brain Health in an Aging Society," Public Health Reports, vol. 133 (3), pp. 225–229, 2018, doi:10.1177/0033354918763599.

[18] Douglas Arneson, Yong Zhang, Xia Yang and Manikandan Narayanan, "Shared mechanisms among neurodegenerative diseases: from genetic factors to gene networks," Journal of Genetics, vol. 97(3), pp. 795–806, July 2018, doi.org/10.1007/s12041-018-0963-3.

[19] T. Tirupal and B. Chandra Mohan, "Pixel-Level Multifocus Image Fusion based on Wavelet Transform & Principal Component Analysis," Journal of Innovation in Electronics & Communication, vol. 2(2), pp. 60–64, 2012.

[20] E. Jagadeesh and T. Tirupal, "A Multimodal Image Fusion based on Dual Tree Complex 2D-Discrete Wavelet Transform Method," International Journal for Technological Research in Engineering, vol. 2(12), pp. 3151–3156, Aug-2015.

[21] E. Gopi Krishna and T. Tirupal, "Performance of Image Fusion Techniques for Satellite Images," International Journal for Technological Research in Engineering, vol. 2(12), pp. 3184–3188, Aug-2015.

[22] Vikrant Bhateja, Aisha Moin, Anuja Srivastava, Le Nguyen Bao, Aime Lay-Ekuakille, and Dac-Nhuong Le, "Multispectral medical image fusion in Contourlet domain for computer based diagnosis of Alzheimer's disease," Review of Scientific Instruments, vol. 87, pp.074303, 2016. doi:10.1063/1.4959559.

[23] T. Tirupal, B. Chandra Mohan and S. Srinivas Kumar, "On the Use of Undecimated Discrete Wavelet Transform for Medical Image Fusion," National Conference on 'Present Scenario and Future Trends in Biomedical Engineering and

Healthcare Technologies', FTBH-2014, IIT BHU, Varanasi, 17-18 October 2014, pp. 5-6.

[24] T. Tirupal, B. Chandra Mohan and S. Srinivas Kumar, "Image Fusion of Natural, Satellite, and Medical Images using Undecimated Discrete Wavelet Transform and Contrast Visibility," IEEE National Conference on Recent Advances in Electronics & Computer Engineering (RAECE), IIT Roorkee, India, pp. 11–16, Feb 2015, doi:10.1109/RACE.2015.7510217.

[25] T. Tirupal, "Multifocus image fusion based on segmentation using stationary wavelet transform", International Journal of Trend in Research and Development (IJTRD), Special Issue RIET-2017, December 2017.

[26] P. Praneel Kumar, K. Madhavi and T. Tirupal, "Multimodal Medical Image Fusion based on Undecimated Wavelet Transform and Fuzzy Sets," International Journal of Innovative Technology and Exploring Engineering, vol. 8(6), April 2019.

[27] T. Tirupal, B. Chandra Mohan and S. Srinivas Kumar, "Medical Image Fusion using UDWT, Fuzzy Sets and Optimization Techniques," Published by 'LAP LAMBERT Academic Publishing', Germany, ISBN 978-620-0-22682-2 on 2nd July 2019.

[28] T. Tirupal, B. Chandra Mohan and S. Srinivas Kumar, "Multifocus Medical Image Fusion based on Fractional Lower Order Moments and Modified Spatial Frequency," International Conference on Advances in Biotechnology, BIOTECH-2015, IIT Kanpur, India, 13-15 March 2015, pp.145-154.

[29] T. Tirupal, B. Chandra Mohan and S. Srinivas Kumar, "Type-2 Fuzzy Set based Multimodal Medical Image Fusion," Indian Conference on Applied Mechanics (INCAM-2019), IISc Bangalore, India, 03-05 July, 2019.

[30] G. Mahalaxmi and T. Tirupal, "Detection of Lung Cancer Using Binarization Technique," IUP Journal of Information Technology, vol. 13(4), pp. 7–19, Dec 2017.

[31] Md. Mahaboob Basha and T. Tirupal, "On the Use of Spatial Frequency Technique for Detection of Brain Tumors in Medical Images," International Journal for Technological Research in Engineering, vol. 2(12), pp. 3169–3174, Aug-2015.

[32] T. Tirupal, B. Chandra Mohan and S. Srinivas Kumar, "Multimodal Medical Image Fusion based on Yager's Intuitionistic Fuzzy Sets," Iranian Journal of Fuzzy Systems, vol. 16(1), 2019, pp. 33–48, doi:10.22111/IJFS.2019.4482.

[33] T. Tirupal, B. Chandra Mohan and S. Srinivas Kumar, "Multimodal Medical Image Fusion based on Sugeno's Intuitionistic Fuzzy Sets," ETRI Journal, vol. 39(2), pp.173–180, 2017, doi.org/10.4218/etrij.17.0116.0568.

[34] T. Tirupal, B. Chandra Mohan, S. Srinivas Kumar, "Multimodal Medical Image Fusion based on Fuzzy sets with Orthogonal Teaching–Learning-Based Optimization," In: Verma N., Ghosh A. (eds) Computational Intelligence: Theories, Applications and Future Directions – Volume II. Advances in Intelligent Systems and Computing, vol 799, october 2018, Springer, Singapore, doi.org/10.1007/978-981-13-1135-2_37.

[35] T. Tirupal and B. Chandra Mohan, "A Fusion Method for Multimodal Medical Images Based on Fuzzy Sets with Teaching Learning Based Optimization", International Conference on Advances in Scientific Computing, IIT Madras, Chennai, India, 28-30 November, 2016.

[36] K. Gayathri and T. Tirupal, "Multimodal Medical Image Fusion based on Type-1 Fuzzy Sets," Journal of Applied Science and Computations, vol. 5(10), pp. 1329–1341, 2018.

[37] H. Nikhat Afreen and T. Tirupal, "Multimodal Medical Image Fusion Based on Fuzzy Enhancement and Fuzzy Transform," International Journal of Research, vol. 5(4), pp. 3002–3010, February 2018.

[38] B. Renuka Devi and T. Tirupal, "Image fusion using Teaching Learning based Optimization", Elixir International Journal – Elixir Digital Processing, vol. 96, pp. 41229–41231, July-2016.

[39] A. Das and M. Bhattacharya, "Effective image fusion method to study Alzheimer's disease using MR, PET images," in Proceedings of the IEEE International Conference on Bioinformatics and Biomedicine, pp. 1603–1607, 2015.

[40] Donghuan Lu, Karteek Popuri, Weiguang Ding, Rakesh Balachandar, Mirza Faisal Beg, "Multimodal and Multiscale Deep Neural Networks for the Early Diagnosis of Alzheimer's Disease using structural MR and FDG-PET images," 2017, arXiv:1710.04782v1.

[41] M. Paul Murphy, "Amyloid-Beta Solubility in the Treatment of Alzheimer's Disease," The New England Journal of Medicine, vol. 378 (4), January 25, 2018, doi:10.1056/NEJMe1714638.

[42] A. Eskicioglu, P. Fisher, "Image quality measures and their performance," IEEE Transactions on Communications, vol. 43(12), pp. 2959–2965, 1995.

[43] P. Jagalingam, A. V. Hegde, "A review of quality metrics for fused image," Aquatic Procedia, vol. 4, pp. 133–142, 2015.